82-1010

Diffractive Anisoplanatism and Tracker Bandwidth Limitations

S.E.J. Shaw
E.M. Tomlinson

26 September 2018

Lincoln Laboratory
MASSACHUSETTS INSTITUTE OF TECHNOLOGY
LEXINGTON, MASSACHUSETTS

This material is based upon work supported by the Joint Directed Energy Transition Office (DE-JTO) under Air Force Contract No. FA8721-05-C-0002 and/or FA8702-15-D-0001.

This report is the result of studies performed at Lincoln Laboratory, a federally funded research and development center operated by Massachusetts Institute of Technology. This material is based upon work supported by the Joint Directed Energy Transition Office (DE-JTO) under Air Force Contract No. FA8721-05-C-0002 and/or FA8702-15-D-0001. Any opinions, findings, conclusions or recommendations expressed in this material are those of the author(s) and do not necessarily reflect the views of the Joint Directed Energy Transition Office.

Massachusetts Institute of Technology
Lincoln Laboratory

Diffractive Anisoplanatism and Tracker Bandwidth Limitations

S.E.J. Shaw
E.M. Tomlinson
Group 82

Special Report No. 82-1010

26 September 2018

Lexington Massachusetts

This page intentionally left blank.

EXECUTIVE SUMMARY

This report develops the concept of "diffractive anisoplanatism," a previously omitted effect that places fundamental limitations on tracker performance for directed-energy applications. Diffractive anisoplanatism comprises two effects: first, that diffraction causes the conversion of phase to amplitude on the beacon light used to drive a tracker, effectively hiding some atmospheric phase from tilt measurements; second, that diffraction causes a scoring beam propagating to the target to spread into regions outside of the geometric cone sampled by the beacon. These two effects result in a loss of reciprocity between the two beams, such that using the beacon tilt to correct the scoring-beam motion will not drive that motion to zero as conventional wisdom would dictate. This is true even in an idealized situation with no spatial offsets, no latency, no noise or errors, infinite bandwidth, and no time-of-flight delays. Further, this loss of reciprocity worsens as frequency increases, such that our attempts to correct scoring-beam jitter above a scenario-dependent frequency f_{S} will actually make the jitter on target worse.

The research that lead to this analysis of diffractive anisoplanatism was motivated by the "v/D problem," an observation in the literature of an upper limit to useful tracker bandwidth. There are a number of potential considerations for tracker design that might place an upper limit on bandwidth, including diminishing returns and tracker noise at high frequencies. Diffractive anisoplanatism provides a fundamental physics limit that should be considered alongside these practical limitations.

This page intentionally left blank.

TABLE OF CONTENTS

This page intentionally left blank.

LIST OF FIGURES

This page intentionally left blank.

1. INTRODUCTION

An ideal tracking scenario would place a point-source beacon at the desired aim point, operating at the same wavelength and measured in the same aperture as the scoring beam. If beacon tilt measurements were free of noise and error, if we could ignore the travel time of photons along the path, and if corrections could be applied to the scoring beam with infinite bandwidth and zero latency, then conventional wisdom would dictate that we could drive the scoring-beam jitter to zero. This conclusion is based on an assumption of perfect reciprocity between the beacon tilts and scoring-beam motion in the target plane; our tracker must rely on this reciprocity, as it has no direct knowledge of the scoring-beam motion in the target plane. In this report, we develop the concept of "diffractive anisoplanatism" and show that it causes a loss of reciprocity between these beams, even in this idealized scenario.[1]

It is well established that anisoplanatic effects can limit the performance of tracking and adaptive-optics corrections of atmospheric turbulence. The scenario described above, however, was specifically designed to eliminate all of the usual sources of anisoplanatism. Previous publications have described an observed upper limit to useful tracker bandwidth, even in geometries approaching this ideal [1–4]. That bandwidth limit has been seen to scale with the wind speed divided by the aperture diameter, and the idea of a "v/D problem" has arisen in the tracking literature, most notably in the work of Dr. Paul Merritt. These previous studies, discussed in more detail in §4, have hypothesized that this phenomenon can be attributed to a combination of measurement noise and the decreasing tilt content of spatial wavelengths shorter than the aperture. This noise-driven loss of reciprocity presents a practical limitation that may dominate diffractive ansiplanatism but could in principle be avoided; this research was motivated by a desire to identify additional, fundamental limits to reciprocity.

Diffractive anisoplanatism arises from inescapably different sampling of the atmosphere by a point-source beacon and a scoring beam propagating to the target. We will demonstrate this analytically, first with a simple sinusoidal phase profile and then for full atmospheric turbulence, showing that it results in uncorrectable residual jitter and a fundamental upper limit f_{S} on useful tracker bandwidth, even for an idealized system. Though only one of a number of factors that may limit useful bandwidth, we believe that f_{S} is an important parameter to consider in tracker design.

This report draws heavily on the analytical methods developed in a previous report to the DE-JTO [5]. Relevant results will be cited and used here, but, because our focus here is the physical conclusions about diffractive anisoplanatism, we will not go through the full derivations. Please refer to the previous report for a detailed treatment on developing these kinds of analytic expressions for atmospheric propagation statistics.

[1] Though the term "diffractive anisoplanatism" was used qualitatively by Enguehard and Hatfield in a discussion of adaptive optics (see, e.g., "Introduction to laser guide star theory versus experiment," Proc. SPIE 5895, 2005), the similarity with this work ends with the observation that diffraction can affect reciprocity.

This page intentionally left blank.

2. DIFFRACTIVE ANISOPLANATISM

Anisoplanatism arises between two beams that sample the atmosphere differently. Three familiar forms of anisoplanatism arise when beams have lateral, angular, or temporal offsets from one another – examples which can all be understood with simple ray-optics pictures (e.g., [6, Figs. 3.7, 5.2, and 5.3]). Diffractive anisoplanatism differs in that it requires us to look beyond the ray-optics limit of propagation. The two relevant effects, illustrated in Figure 1, are the loss of phase information on the beacon light as diffraction converts phase to amplitude, and the diffractive spreading of the scoring beam outside of the cone of light sampled by the beacon. We will treat the beacon light as coming from an ideal point source at the aim point, which could be a cooperative beacon, a retroreflector, or a glint. In this section, we will develop the equations necessary to show the relevant differences between beacon tilt and scoring-beam centroid motion.

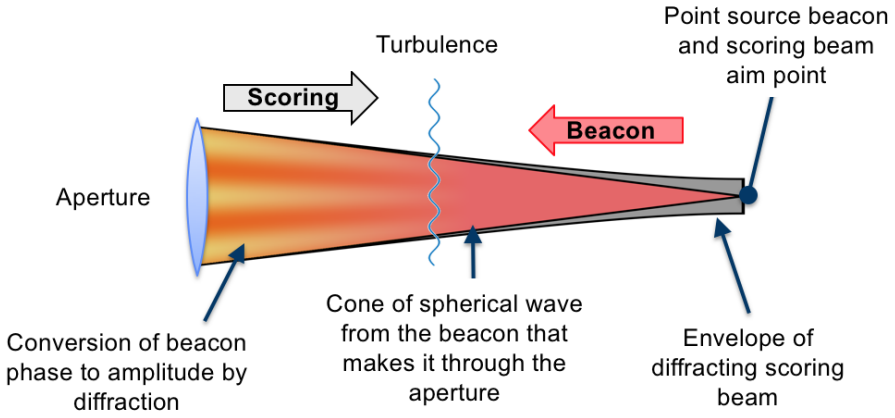

Figure 1. Illustration of the propagation of point-source beacon light to an aperture (red cone) and a scoring beam to the target plane (grey region), showing the two diffractive effects that lead to anisoplanatism. First is the conversion of beacon phase into amplitude, indicated by a change in color from red to yellow, which results in a loss of phase information on the beacon light. Second is the spreading of the focused scoring beam outside of the cone sampled by the beacon, spoiling the geometric overlap of the two beams.

2.1 DIFFRACTIVE ANISOPLANATISM WITH A SINUSOIDAL PHASE PROFILE

Our ultimate goal in analyzing diffractive anisoplanatism is to make a comparison between the tilts present on beacon light in the receive aperture and the centroid motion of the scoring beam in the target plane after both beams have propagated through the atmosphere. Following the techniques developed in [5], we will build up to this by first considering the effect of a single sinusoidal phase profile at position z along the path, with transverse wave vector $\boldsymbol{\kappa}$ and real-valued

phase $\alpha(\boldsymbol{\kappa}, z)$. Our normalized phase profile[2] at transverse position $\mathbf{r}$ and time t is given by

$$\phi(\boldsymbol{\kappa}, \mathbf{r}, z, t) = \sin\left[\boldsymbol{\kappa} \cdot \mathbf{r} + \alpha(\boldsymbol{\kappa}, z) - \boldsymbol{\kappa} \cdot \mathbf{v}(z)t\right] . \tag{1}$$

We have included a time-dependent phase offset, consistent with the frozen-turbulence hypothesis, to move our phase profile through the beam with constant velocity $\mathbf{v}(z)$.

For a scoring beam propagating from 0 to L, assuming a circularly-symmetric irradiance profile $a^2(r, z)$ and total power P, the phase profile in Eq. 1 causes a centroid motion in the target plane of [5, Eq. 52]

$$\frac{1}{L} X_m(\boldsymbol{\kappa}, z, t; L) = \frac{(L-z)\kappa}{Lk} \cos\left[\alpha(\boldsymbol{\kappa}, z) - \boldsymbol{\kappa} \cdot \mathbf{v}(z)t\right] \cos(\varphi_m - \varphi_\kappa) \mathcal{F}\left[\frac{a^2(r, z)}{P}\right] , \tag{2}$$

where $\mathcal{F}$ denotes a two-dimensional Fourier transform and k is the wave number of the propagating field. In Eq. 2, we measure the component of centroid motion in the $\hat{\mathbf{m}}$ direction, with $\hat{\mathbf{m}}$ and $\boldsymbol{\kappa}$ at angles φ_m and φ_κ from the $\hat{\mathbf{x}}$ axis, and the division by L gives us jitter in radians using a small-angle approximation. Eq. 2 was derived using the centroid tilt (C tilt) on the beam, the irradiance-weighted gradient of the field. There is a mathematical equivalence between the irradiance-weighted gradient of a field and the irradiance centroid of its Fourier transform, making C tilt, rather than the more familiar gradient and Zernike tilts (G and Z tilts), the quantity directly related to target-plane centroid jitter [5, §4].

Tracking systems can be designed to respond to either the G tilt or the Z tilt on the incoming beacon light. Because the C tilt that determines scoring-beam centroid motion is more closely related to G tilt, we expect greater reciprocity if we use G tilt for tracking. To demonstrate this difference, we consider expressions for both. The sinusoidal phase profile in Eq. 1 results in a G tilt measurement in the aperture of [5, Eq. 8]

$$\theta_{\mathrm{G},m}(\boldsymbol{\kappa}, z, t; 0) = \frac{4}{kD_{\mathrm{B}}(0)} \cos\left[\alpha(\boldsymbol{\kappa}, z) - \boldsymbol{\kappa} \cdot \mathbf{v}(z)t\right] \cos(\varphi_m - \varphi_\kappa) \cos\left(\frac{\kappa^2 D_{\mathrm{B}}(z) z}{2kD_{\mathrm{B}}(0)}\right) J_1\left(\frac{D_{\mathrm{B}}(z)\kappa}{2}\right) , \tag{3}$$

where J_1 is a Bessel function of the first kind. This expression is for a point-source beacon propagating from L to 0, tracing out a cone of diameter $D_{\mathrm{B}}(z) = D(1 - z/L)$ to an aperture of diameter D, as shown in Figure 1. As with C tilt, we measure G tilt in the $\hat{\mathbf{m}}$ direction. If instead of G tilt we measure the Z tilt, we have [5, Eq. 33]

$$\begin{aligned}\theta_{\mathrm{Z},m}(\boldsymbol{\kappa}, z, t; 0) = \frac{32}{k\kappa D_{\mathrm{B}}(z) D_{\mathrm{B}}(0)} &\cos\left[\alpha(\boldsymbol{\kappa}, z) - \boldsymbol{\kappa} \cdot \mathbf{v}(z)t\right] \cos(\varphi_m - \varphi_\kappa) \cos\left(\frac{\kappa^2 D_{\mathrm{B}}(z) z}{2kD_{\mathrm{B}}(0)}\right) \\ &\times J_2\left(\frac{D_{\mathrm{B}}(z)\kappa}{2}\right) .\end{aligned} \tag{4}$$

The third cosine term that appears for both G and Z tilts gives us the diffractive conversion of phase to amplitude, and is notably missing from the centroid jitter expression.

[2] The expressions that will follow are linear in the amplitude of this phase, so we will work with a normalized phase and omit the small-amplitude multiplier implicit in the theory.

Because Eq. 2 depends on the details of the irradiance profile $a^2(r,z)$, direct comparison with Eqs. 3 and 4 is nontrivial. Whatever the details of the propagating scoring beam, we can define some beam diameter $D_{\mathrm{S}}(z)$ as a function of position along the path and approximate the field with a flat irradiance profile of that diameter. With this simplification, we can evaluate the transform in Eq. 2, giving

$$\frac{1}{L}X_m(\boldsymbol{\kappa},z,t;L) = \frac{4(L-z)}{LkD_{\mathrm{S}}(z)}\cos\left[\alpha(\boldsymbol{\kappa},z) - \boldsymbol{\kappa}\cdot\mathbf{v}(z)t\right]\cos(\varphi_m-\varphi_\kappa)J_1\left(\frac{D_{\mathrm{S}}(z)\kappa}{2}\right). \tag{5}$$

This is a ray-optics approximation to the beam profile, but it allows us to mimic diffractive spreading by setting $D_{\mathrm{S}}(z) > D_{\mathrm{B}}(z)$, as indicated schematically with the grey region in Figure 1. The result is very similar to the expression for beacon G tilt in Eq. 3.

Equations 3, 4, and 5 have identical time dependence in a shared cosine term, and are therefore perfectly correlated and coherent with one another. To the extent that their amplitudes differ, however, reciprocity is broken. Plots of these three equations, with the shared cosine terms removed, are shown in Figure 2. The x axes are the dimensionless quantity $D_{\mathrm{B}}(z)\kappa$, which is equal to 2π for a sinusoidal phase profile with wavelength equal to $D_{\mathrm{B}}(z)$. These curves show that, for long spatial wavelengths ($D_{\mathrm{B}}(z)\kappa \ll 2\pi$), all three measurements are the same and we have good reciprocity. As the spatial wavelength gets shorter ($D_{\mathrm{B}}(z)\kappa \gtrsim 2\pi$), first Z tilt, then G tilt diverge from the scoring-beam jitter measurement, due to the conversion of beacon phase to amplitude. At a given wind speed, larger values of κ correspond to higher temporal frequencies, so we would expect to see worse reciprocity at high frequencies. Not only do the tilt measurements have different magnitudes than the centroid motion, for some κ values they have different signs. If we include spreading of the scoring beam due to diffraction, allowing $D_{\mathrm{S}}(z) > D_{\mathrm{B}}(z)$ with the top-hat-profile simplification of Eq. 5, small differences in the sizes of the beams mean a loss of reciprocity at even smaller values of $D_{\mathrm{B}}(z)\kappa$; the fact that the scoring beam does not remain a top hat as it propagates would further reduce reciprocity.

There are a few additional insights that we can take away from the plots in Figure 2. As we move from the center of these plots to the edges, either towards larger or smaller $D_{\mathrm{B}}(z)\kappa$, we see the amplitude of tilts decreasing. The amplitude of the sinusoidal phase profile being applied is constant, so this observation reflects a κ-dependent decrease in the tilt content of the sinusoidal phase: when $D_{\mathrm{B}}(z)\kappa \ll 2\pi$, the wavelength of the phase is much larger than D and the phase looks flat over the aperture; when $D_{\mathrm{B}}(z)\kappa \gg 2\pi$, the phase has many periods over the aperture and contributes mostly to higher-order modes rather than to tilt. The peak in tilt content is near $D_{\mathrm{B}}(z)\kappa \sim 2\pi$, where the turbulence wavelength is close to the aperture diameter. Further, if there is a cross wind of velocity $v(z)$, then the frequency with which our tilt will change is given by $v(z)\kappa/2\pi$, so this peak in tilt comes at a frequency around $v(z)/D_{\mathrm{B}}(z)$. This is related to diminishing returns to tilt correction above v/D, which we will discuss in §4.

2.2 DIFFRACTIVE ANISOPLANATISM WITH ATMOSPHERIC TURBULENCE

In the previous section, we demonstrated with simple sinusoidal phase profiles that reciprocity worsens at high frequencies. For a more relevant illustration of this, we can look at the power

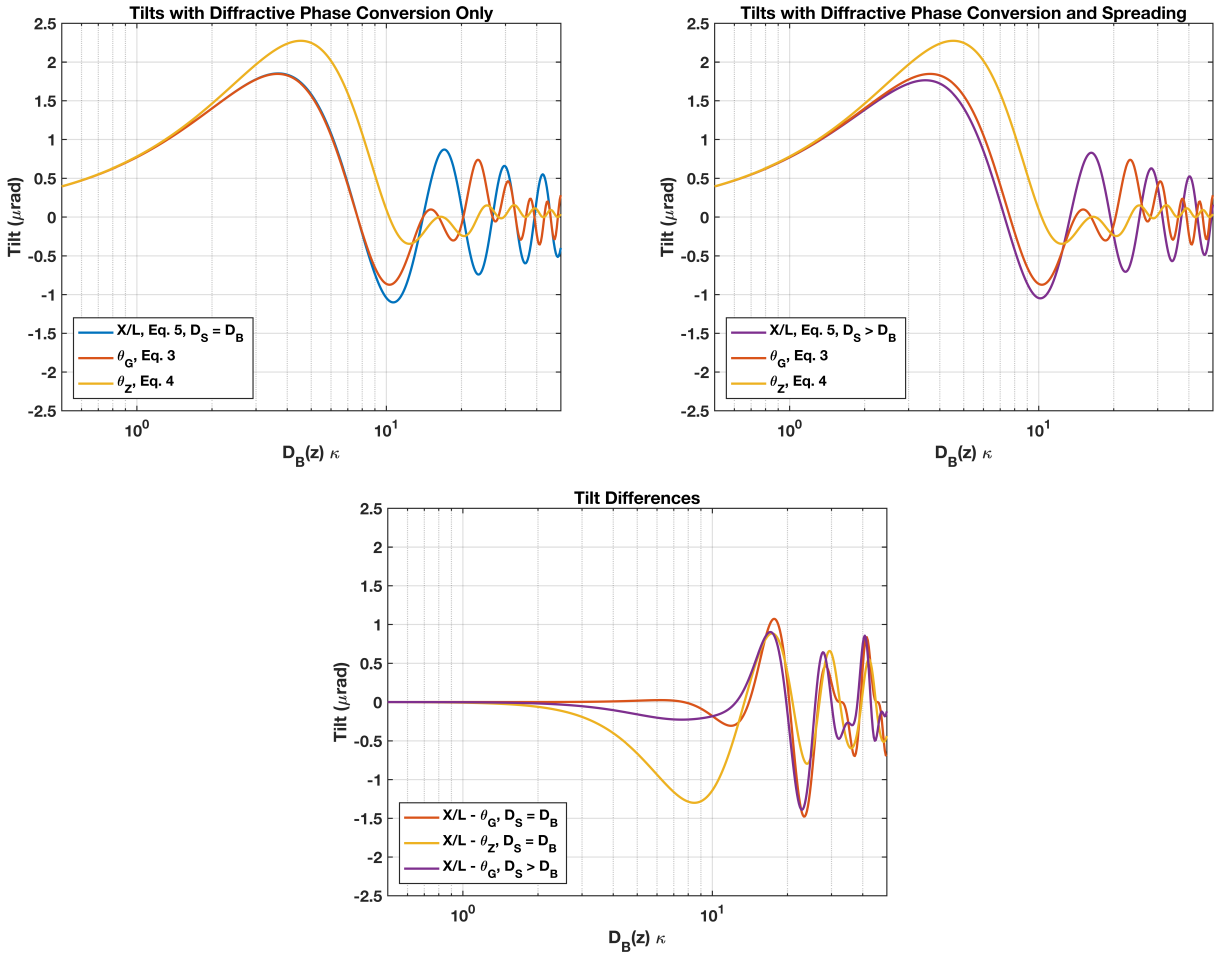

Figure 2. These plots illustrate the breakdown of reciprocity between beacon G tilt and Z tilt and scoring-beam centroid motion, all due to a single sinusoidal phase profile. The plots are of Eqs. 3, 4, and 5, with the shared cosine terms removed because all three signals have identical time dependence. Our sinusoidal phase profile has unit amplitude and is placed at the midpoint of a 3 km path, the fields have 1 μm wavelengths, and we have a 20 cm aperture. On the top left we show a comparison with $D_{\rm S}(z) = D_{\rm B}(z)$, so the loss of reciprocity is due entirely to diffractive conversion of beacon phase to amplitude. On the top right, we take $D_{\rm S}(z) = 1.05 D_{\rm B}(z)$ to simulate the effect of diffractive spreading of the scoring beam. On the bottom, we take the differential tilts to show how the measurements increasingly differ in magnitude, sometimes in sign, as κ increases.

spectral densities (PSDs) of the beacon G tilt and scoring-beam centroid jitter for propagation through full atmospheric turbulence; because of the clearly worse reciprocity seen for Z tilt,[3] we will focus on tracking with G tilt. Given the expressions for the centroid motion and beacon tilt due to a single sinusoidal phase profile, it is straightforward to calculate variances and PSDs for propagation through the atmosphere. First, we need the variances found by ensemble averaging our tilts over $\alpha(\boldsymbol{\kappa}, z)$, assuming uniform distribution of this random phase, with Eq. 2 giving us

$$\sigma^2_{X/L,m}(\boldsymbol{\kappa}, z; L) = \frac{(L-z)^2\kappa^2}{2L^2k^2}\cos^2\left(\varphi_m - \varphi_\kappa\right)\left\{\mathcal{F}\left[\frac{a^2(r,z)}{P}\right]\right\}^2 \tag{6}$$

for centroid jitter, and Eq. 3 giving us

$$\sigma^2_{\mathrm{G},m}(\boldsymbol{\kappa}, z; 0) = \frac{8}{k^2 D^2_{\mathrm{B}}(0)}\cos^2\left(\varphi_m - \varphi_\kappa\right)\cos^2\left(\frac{\kappa^2 D_{\mathrm{B}}(z) z}{2k D_{\mathrm{B}}(0)}\right) J_1^2\left(\frac{D_{\mathrm{B}}(z)\kappa}{2}\right) \tag{7}$$

for G tilt. Because both the beacon tilt and the scoring-beam centroid motion are linear calculations in the phase being applied, we can build up the combined effects of atmospheric turbulence by integrating these single-sinusoid variances along the atmospheric channel. We have

$$\sigma^2_m = 4\pi k^2 \int_0^L dz\, C_n^2(z) \int_0^\infty d\kappa\, \kappa\, \Phi_n^0(\kappa) \int_0^{2\pi} d\varphi_\kappa\, \sigma^2_m(\boldsymbol{\kappa}, z; L)\,, \tag{8}$$

where the inner σ^2_m term can be replaced with either of the variances above, $\Phi_n^0(\kappa)$ is the power spectrum of atmospheric turbulence (e.g., Kolmogorov or von Karman turbulence), and $C_n^2(z)$ gives the strength of turbulence along the path [5, Eq. 12].

From the path-integrated variance in Eq. 8 we can get a PSD in frequency f via a change in variables [5, §2.5],

$$\kappa = \frac{2\pi f}{v(z)\cos(\varphi_f)} \quad \text{and} \quad \varphi_f = \varphi_\kappa - \varphi_v(z)\,, \tag{9}$$

where $\varphi_v(z)$ is the angle of $\mathbf{v}(z)$. These variables together give us the one-sided PSD expression

$$\begin{aligned}\mathrm{PSD}_m(f) = 32\pi^3 k^2 f \int_0^L dz\, C_n^2(z) v^{-2}(z) \int_{-\pi/2}^{\pi/2} d\varphi_f\, \sec^2(\varphi_f) \Phi_n^0\left(\frac{2\pi f}{v(z)\cos(\varphi_f)}\right) \\ \times \sigma^2_m\left[\frac{2\pi f}{v(z)\cos(\varphi_f)}, \varphi_f + \varphi_v(z), z; L\right]\,.\end{aligned} \tag{10}$$

Substituting $\sigma^2_{X/L,m}$ from Eq. 6 for scoring-beam centroid jitter gives us

$$\begin{aligned}\mathrm{PSD}_{X/L,m}(f) = \frac{10(2\pi)^{1/3}}{9\Gamma\left(\frac{1}{3}\right)} f^{-2/3} \int_0^L dz\, C_n^2(z) v^{-1/3}(z) \left(1 - \frac{z}{L}\right)^2 \int_{-\pi/2}^{\pi/2} d\varphi_f\, \cos^{-1/3}(\varphi_f) \\ \times \cos^2\left[\varphi_m - \varphi_f - \varphi_v(z)\right]\left\{\mathcal{F}\left[\frac{a^2(r,z)}{P}\right]\right\}^2\,,\end{aligned} \tag{11}$$

[3] The inclusion of higher-order adaptive optics (AO) would change this picture somewhat. The difference between G and Z tilts is that all orders of Zernike coma contribute to G tilt but not to Z tilt; if an AO system were to separately correct those higher-order modes, then the difference between G-tilt and Z-tilt would disappear. The other effects that AO would have on beam shape do not affect centroid jitter or tilt measurement.

where Γ is the gamma function and we have assumed Kolmogorov turbulence given by $\Phi_n^0(\kappa) = [5/18\pi\Gamma(\frac{1}{3})]\kappa^{-11/3}$. In practice, we will assume sufficiently weak turbulence that we can approximate $a(r,z)$ with the field profiles found under vacuum propagation. Substituting $\sigma^2_{\mathrm{G},m}$ from Eq. 7 for beacon G tilt gives us

$$\mathrm{PSD}_{\mathrm{G},m}(f) = \frac{80}{2^{2/3}9\pi^{5/3}\Gamma\left(\frac{1}{3}\right)} D_{\mathrm{B}}^{-2}(0) f^{-8/3} \int_0^L dz\, C_n^2(z) v^{5/3}(z) \int_{-\pi/2}^{\pi/2} d\varphi_f\, \cos^{5/3}(\varphi_f)$$
$$\times \cos^2\left[\varphi_m - \varphi_f - \varphi_v(z)\right] \cos^2\left[\frac{D_{\mathrm{B}}(z) z}{2k D_{\mathrm{B}}(0)} \left(\frac{2\pi f}{v(z)\cos(\varphi_f)}\right)^2\right] J_1^2\left(\frac{\pi f D_{\mathrm{B}}(z)}{v(z)\cos(\varphi_f)}\right). \tag{12}$$

In Figure 3, we compare our analytic expressions for $\mathrm{PSD}_{\mathrm{G},m}$ and $\mathrm{PSD}_{X/L,m}$ to each other and to results from wave-optics simulations. The analytic curves agree well with wave optics over all frequencies. Though the analytic PSDs are indistinguishable from one another on these plots at low frequencies, small differences there may contribute to residual jitter given their relatively high magnitude. Because the beacon G tilt has more power at high frequencies than the scoring beam, applying the beacon tilt as a correction to the scoring beam would necessarily increase the scoring beam jitter at those frequencies.

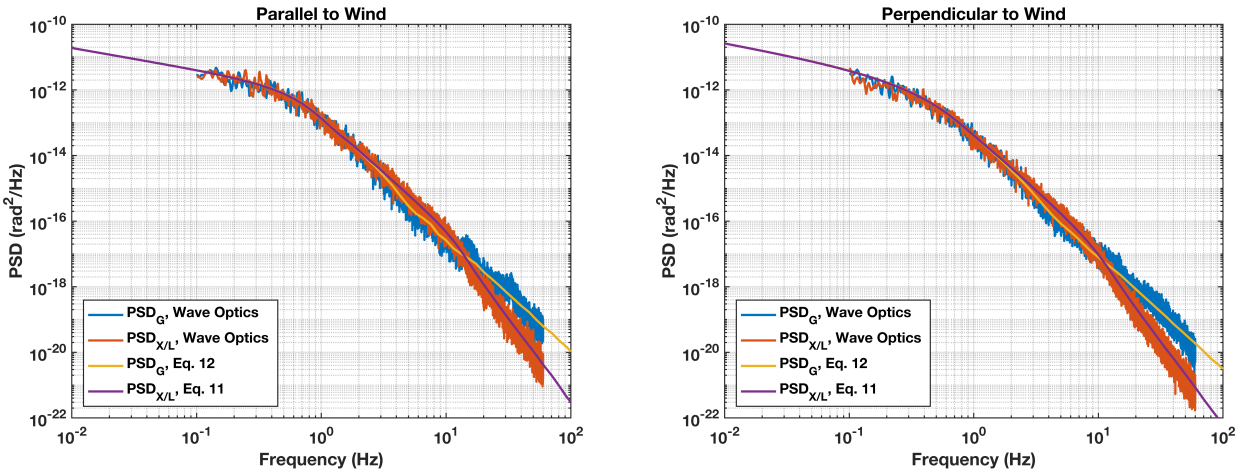

Figure 3. This plot shows a comparison between the PSDs calculated with our analytic expressions for scoring-beam centroid jitter in Eq. 11 and beacon G tilt in Eq. 12, as well as results of wave-optics modeling. The theoretical curves agree well with wave optics, and both show the predicted disagreement between beacon and scoring beam at high frequencies. The scenario chosen was propagation over a 3-km path with a constant 0.2-m/s cross wind, Rytov variance of 0.01, constant C_n^2, and Kolmogorov turbulence. The scoring beam is a 20-cm-diameter top-hat beam at 1-micron wavelength, and the beacon is a point source at the same wavelength and measured in the same aperture. With these parameters, the characteristic frequency v/D is 1 Hz.

3. IMPLICATIONS FOR TRACKER PERFORMANCE

As we developed in the previous section, the result of diffractive anisoplanatism will be a reduction in our ability to correct the scoring beam using tilt measurements from a point-source beacon. To find the residual jitter for a tracking system with no measurement errors or latency, we apply the beacon tilt measurements as corrections to the scoring beam by directly subtracting the measured tilt from the scoring-beam motion. The tracker described here does not have any direct knowledge of the scoring-beam motion, but instead relies on the assumption of reciprocity between the two quantities: without *a priori* knowledge of any differences between the two quantities, this subtraction as a correction is the best that one could do. The difference between Eqs. 2 and 3,

$$\theta_{X/L-\mathrm{G},m}(\boldsymbol{\kappa}, z; L) = \frac{1}{L} X_m(\boldsymbol{\kappa}, z; L) - \theta_{\mathrm{G},m}(\boldsymbol{\kappa}, z; 0)\,, \tag{13}$$

gives the differential jitter resulting from a single sinusoidal phase profile in the path. The ensemble-average variance of Eq. 13 yields

$$\sigma^2_{X/L-\mathrm{G},m}(\boldsymbol{\kappa}, z; L) = \frac{(L-z)^2}{2k^2L^2}\cos^2(\varphi_\kappa - \varphi_m)\left\{\kappa\mathcal{F}\left[\frac{a^2(r,z)}{P}\right] - \frac{4}{D_{\mathrm{B}}(z)}\cos\left(\frac{\kappa^2 D_{\mathrm{B}}(z) z}{2kD_{\mathrm{B}}(0)}\right) J_1\left(\frac{D_{\mathrm{B}}(z)\kappa}{2}\right)\right\}^2, \tag{14}$$

which can be used with Eqs. 8 and 10 to get the path-integrated differential jitter variance and PSD for atmospheric turbulence, respectively.

3.1 RESIDUAL JITTER VARIANCE

One measure of the severity of an anisoplanatic effect is the jitter that remains after we make our correction. Substituting Eq. 14 into Eq. 8 gives us the variance of the differential jitter,

$$\sigma^2_{X/L-\mathrm{G},m} = \frac{5\pi}{9\Gamma\left(\frac{1}{3}\right)}\int_0^L dz\, C_n^2(z)\left(1-\frac{z}{L}\right)^2 \int_0^\infty d\kappa\, \kappa^{-8/3} \times \left\{\kappa\mathcal{F}\left[\frac{a^2(r,z)}{P}\right] - \frac{4}{D_{\mathrm{B}}(z)}\cos\left(\frac{\kappa^2 D_{\mathrm{B}}(z) z}{2kD_{\mathrm{B}}(0)}\right) J_1\left(\frac{D_{\mathrm{B}}(z)\kappa}{2}\right)\right\}^2. \tag{15}$$

We can compare this result to the expressions for the uncorrected centroid jitter variance found using Eqs. 2 and 8,

$$\sigma^2_{X/L,m} = \frac{5\pi}{9\Gamma\left(\frac{1}{3}\right)}\int_0^L dz\, C_n^2(z)\left(1-\frac{z}{L}\right)^2 \int_0^\infty d\kappa\, \kappa^{-2/3}\left\{\mathcal{F}\left[\frac{a^2(r,z)}{P}\right]\right\}^2, \tag{16}$$

and the beacon G tilt found using Eqs. 3 and 8,

$$\sigma^2_{\mathrm{G},m} = \frac{80\pi}{9\Gamma\left(\frac{1}{3}\right) D_{\mathrm{B}}^2(0)}\int_0^L dz\, C_n^2(z)\int_0^\infty d\kappa\, \kappa^{-8/3}\cos^2\left(\frac{\kappa^2 D_{\mathrm{B}}(z) z}{2kD_{\mathrm{B}}(0)}\right) J_1^2\left(\frac{D_{\mathrm{B}}(z)\kappa}{2}\right). \tag{17}$$

Figure 4 shows a comparison between these three quantities as a function of Fresnel number, given by $N_F = (D/2)^2/L\lambda$ where λ is the wavelength of our light; we have varied Fresnel number by changing the aperture diameter. We see that the differential jitter decreases as Fresnel number increases, reducing the effects of diffractive anisoplanatism. The uncorrected scoring-beam jitter and beacon G tilt have very similar variances, and again only differ at low Fresnel number where diffraction is more prominent.

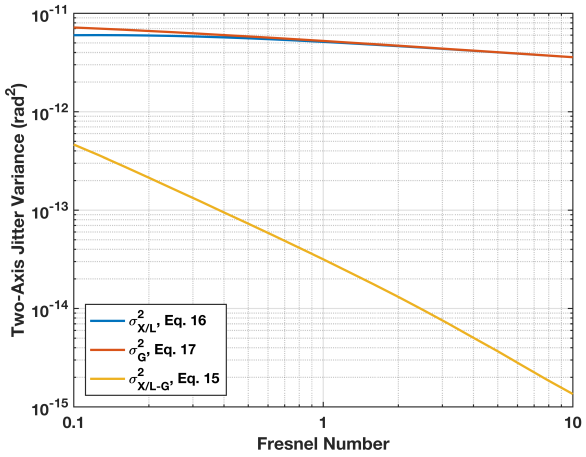

Figure 4. In this plot we compare the variance of differential jitter in Eq. 15 to the scoring-beam centroid jitter and beacon G tilt in Eqs. 16 and 17. The calculations were performed for the same scenario used in Figure 3, except that the aperture diameter was varied to change the Fresnel number of the propagation.

For anisoplanatic effects, it is typically obvious what parameter we can adjust to reduce the severity of the effect in a given scenario; for example, we would reduce the effects of angular anisoplanatism by reducing the apparent angle between the beacon and the aim point. For diffractive anisoplanatism, the analog is that we can reduce the effect by reducing the importance of diffraction in our scenario, which is why we explored the dependence on Fresnel number in Figure 4. Fresnel number, though, is not a parameter that is easy to modify; the range to target, wavelength of light, and aperture size are typically fixed by other considerations. This means that the residual jitter imposed by diffractive anisoplanatism is largely unavoidable, except for a frequency dependence discussed in the following section.

3.2 TRACKER BANDWIDTH LIMITATION

Analysis of anisoplanatic effects often ends with the calculation of a Strehl ratio or residual variance, as we found for diffractive anisoplanatism in the previous section. However, as highlighted in §2.2, the breakdown in reciprocity that leads to this variance doesn't occur equally at all frequencies. The consequences of this frequency-dependent behavior manifest most clearly in a comparison between the PSDs for differential jitter and uncorrected scoring-beam motion.

We find the PSD of the differential jitter by substituting Eq. 14 into Eq. 10, giving us

$$\begin{aligned}\mathrm{PSD}_{X/L-\mathrm{G},m}(f) = \frac{5}{2^{2/3}9\pi^{5/3}\Gamma\left(\frac{1}{3}\right)} f^{-8/3} \int_0^L dz\, C_n^2(z) v^{5/3}(z) \left(1-\frac{z}{L}\right)^2 \int_{-\pi/2}^{\pi/2} d\varphi_f\, \cos^{5/3}(\varphi_f) \\ \times \cos^2\left[\varphi_m - \varphi_f - \varphi_v(z)\right] \left\{ \frac{2\pi f}{v(z)\cos(\varphi_f)} \mathcal{F}\left[\frac{a^2(r,z)}{P}\right] \right. \\ \left. - \frac{4}{D_{\mathrm{B}}(z)} \cos\left[\frac{D_{\mathrm{B}}(z) z}{2k D_{\mathrm{B}}(0)} \left(\frac{2\pi f}{v(z)\cos(\varphi_f)}\right)^2\right] J_1\left(\frac{\pi f D_{\mathrm{B}}(z)}{v(z)\cos(\varphi_f)}\right) \right\}^2 . \end{aligned} \tag{18}$$

This curve, compared to $\mathrm{PSD}_{X/L,m}$ and $\mathrm{PSD}_{\mathrm{G},m}$ (Eqs. 11 and 12) in Figure 5, bears out our earlier observations about diffractive anisoplanatism. The differential jitter PSD has much less power at low frequencies than the uncorrected jitter PSD, and in that regime we benefit significantly from the correction. At high frequencies, the differential PSD is greater than the uncorrected one, reflecting the fact that our "correction" would actually make the centroid motion worse due to the breakdown of reciprocity between the two signals.

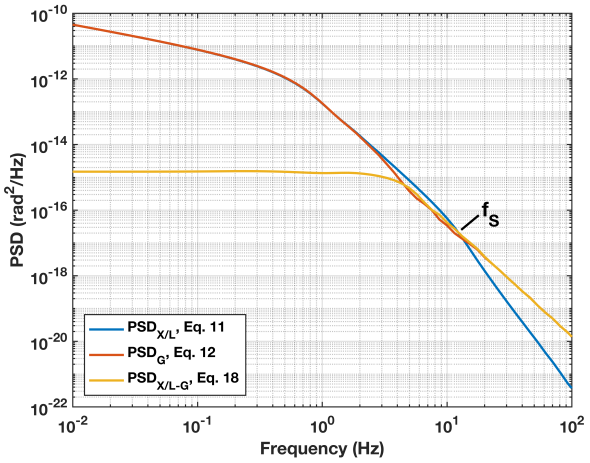

Figure 5. This plot shows the comparison between the PSDs of scoring-beam centroid jitter, beacon G tilt, and the differential jitter between them, calculated for the same scenario used in Figure 3. We show the two-axis jitter, found by summing the PSDs parallel and perpendicular to the wind. We see that there is a frequency $f_{\mathrm{S}} \sim 12$ Hz above which the differential jitter (Eq. 18) has more power than the scoring-beam motion (Eq. 11), meaning corrections above that frequency will increase jitter on target. At frequencies above f_{S}, the red curve (Eq. 12) and yellow curve (Eq. 18) lie on top of one another, and again v/D is equal to 1 Hz.

We have added the x and y PSDs to get the two-axis results, and have labeled the point where those two lines intersect as the scoring-beam crossover frequency f_{S}. This is the maximum frequency at which a tracking system should attempt to correct atmospheric turbulence in this scenario; diffractive anisoplanatism causes corrections above f_{S} to degrade performance. Though one could in principle define separate, directionally-dependent values for f_{S} from the parallel and per-

pendicular PSDs, we have combined them to provide a single value in keeping with other bandwidth considerations such as the Tyler and Greenwood frequencies [7, 8].

By defining f_{S} as the crossing point between two PSDs, we have an implicit definition that, in practice, requires a numeric search. For preliminary assessment, one might prefer an approximate scaling-law expression for f_{S}. For a path with constant v and C_n^2, we can estimate f_{S} with the simple relationship

$$f_{\mathrm{S}} \approx 0.945 \frac{vD}{L\lambda} = 3.78 \frac{v}{D} N_{\mathrm{F}} \,, \tag{19}$$

where N_{F} is the Fresnel number. In Figure 6, we show that this expression gives an estimate of f_{S} with an RMS error of less than 7% over a wide range of geometries. The N_{F} dependence reflects the decreasing importance of diffraction with increasing Fresnel number, and the scaling with v/D arises directly from the $D\kappa$ terms that appear in our PSD expressions. It is important to note, however, that the overall expression for f_{S} scales linearly with D rather than $1/D$, which implies that diffractive anisoplanatism cannot be the underlying mechanism of the previous observations of the v/D problem; rather, it is an additional limitation based on fundamental physics. Another thing to note is that f_{S} is not dependent on the strength of the turbulence; the actual value of C_n^2 does not appear in Eq. 19. The effect of changing C_n^2 uniformly along the path is to shift the PSDs in magnitude, but they shift together so that their crossing point remains unaffected; this will be true as long as we are in a regime where the underlying theory holds, with a Rytov variance $\lesssim 0.4$ [5, §4.4].

Eq. 19 has greater error in estimating f_{S} when C_n^2 and v are allowed to vary along the path, as also shown in Figure 6. The results still follow the trends of our simple scaling law if we replace v with $\max[v(z)]$, and the scaling law allows for a reasonable initial assessment. There are a number of additional effects beyond the scope of this report that could alter the behavior of f_{S}, including modified turbulence statistics (e.g., adding inner and outer scale), extended beacons, conjugating the tilt measurement to a different location along the path, or interactions of the PSDs with realistic tracker error-rejection curves.

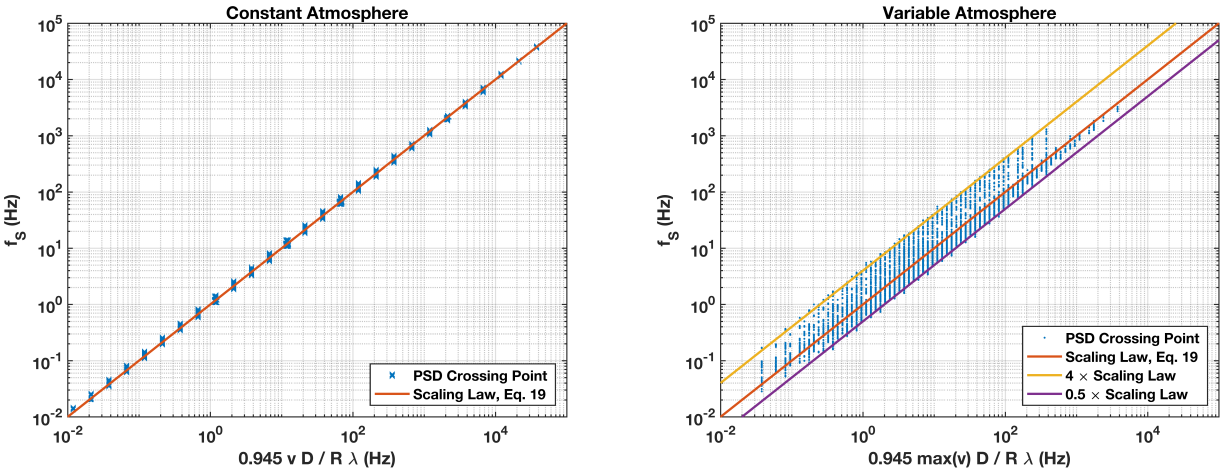

Figure 6. The plot on the left shows the calculated f_S values for a wide range of scenarios with varying aperture size, wind speed, and Fresnel number, with v/D ranging from 0.01 to 100 and Fresnel number ranging from 0.3 to 100, but all with constant C_n^2 and wind speed along the path. We see good agreement with our scaling law over more than six orders of magnitude of f_S, with an RMS error of less than 7%. When we consider cases with variable wind speed (up to 10× along the path) and C_n^2 (up to 100× along the path), or Fresnel numbers less than 0.3, we see deviation from the scaling law; 95% of the cases run lie within the bounds indicated, and still clearly follow the trend of the scaling law when we use the maximum wind speed along the path.

This page intentionally left blank.

4. COMPARISON TO PREVIOUS LITERATURE

This work on diffractive anisoplanatism was initially motivated by a desire to understand the v/D problem, an observation of an upper limit to useful track bandwidth in some directed-energy applications. For reasons outlined above, diffractive anisoplanatism appears to be an independent, fundamental limitation on track bandwidth, which highlights an important point: a number of different effects place upper limits on the useful tracker bandwidth, and the existing literature does not always clearly delineate them. We have found that a useful way to discuss these considerations is to classify them as follows:

	Above some limit, should we reduce jitter any further?	Above some limit, can we reduce jitter by increasing bandwidth?
Practical limitations	Diminishing returns (Siegenthaler [4], Merritt [1–3])	Noise floor (Merritt [1–3])
Fundamental limitations	Centroid anisoplanatism (Yura and Tavis [9])	Diffractive anisoplanatism (this work)

In previous studies, especially experimental observations, it is likely that all four of these effects influenced the results. The dominant effect will be application and scenario dependent, and all of them should be considered in the balance of cost and complexity vs. performance when designing a tracking system.

Because the tilt content of the atmosphere decreases as we increase frequency, at some point it isn't worth the cost or effort to further increase track bandwidth. The diminishing returns for bandwidths above v/D is a combined result of two effects. First is the turbulence spectrum of the atmosphere, which has decreasing power at higher frequencies. Second, as noted in our discussion of Figure 2, is that temporal frequencies above v/D come from short spatial wavelengths of turbulence that contribute primarily to higher-order Zernike modes. This second effect causes the change in slope around v/D for all of the PSDs shown in this paper, and has been known in the literature for many years [10]. Diminishing returns is effectively the aspect of tracking dealt with by Siegenthaler's Z-tilt gain function [4].

As tilt content decreases, there will be some limit beyond which any realistic tracking system is just measuring noise. The noise floor in tracker measurements is related to the decreasing tilt content as frequencies increase, and it makes sense that noise would come to dominate at some frequency close to v/D given the change in slope and rapid falloff of the analytic PSD above that frequency. Noise, however, is a practical hardware limitation and not a feature of the atmosphere. Merritt [3] touches on this topic, in addition to the arguments from Siegenthaler, when he argues that it is hard to make accurate or repeatable measurements of the tilt due to higher spatial frequencies and postulates that the v/D problem is the result of these measurement difficulties. It is also worth noting that Merritt includes results from wave-optics calculations [3, Fig. 7.22] showing perfect coherence between jitter from a top-hat scoring beam and track source tilt measurements when there is no noise. This observation is in complete accord with the results here; the coherence

is expected, but, as mentioned in §2.1, does not in and of itself imply that subtracting one signal from the other will drive the residual to zero.

Centroid anisoplanatism calls into question whether the goal of tracker design should be driving scoring-beam centroid jitter to zero, because doing so can actually increase the long-exposure Strehl ratio of the beam. This is the result of the fact that, in addition to the Zernike tilt term, all orders of Zernike coma contribute to the motion of the beam centroid [9]. Because a tracker uses tilt alone to reduce centroid jitter, we are trying to correct higher-order modes with tilt and as a result will increase the RMS phase error on the beam.

As for fundamental limitations on jitter correction, previous theoretical treatments of tracking have often begun with assumptions that preclude seeing the diffractive anisoplanatism discussed in this paper. Sasiela, for example, assumes that centroid jitter on target arises from Z tilt rather than C tilt and chooses to neglect diffraction in his analysis, thus guaranteeing perfect reciprocity with a Z-tilt-driven tracker [11, §4.7]. Diffractive anisoplanatism results from fundamental properties of propagation that reduce reciprocity between point-source-beacon tilt and scoring-beam jitter. This limits the possibility of reducing jitter by increasing bandwidth, even in an idealized system free of noise or other errors. We find uncorrectable jitter at all frequencies, and in particular there is a limiting frequency f_{s} above which attempted correction will actually increase jitter on target.

5. CONCLUSIONS

In this report, we have described a form of anisoplanatism that has previously been omitted from discussions and analytic treatments of tracking. Diffractive anisoplanatism is the result of two effects: the conversion of phase to amplitude on the beacon light used to drive a tracker, and the spreading of the scoring beam outside of the geometric cone of atmosphere sampled by the beacon. These effects of diffraction lead to a loss of reciprocity between beacon tilt measurements and scoring-beam centroid motion, even in an idealized tracking scenario specifically constructed to avoid previously treated anisoplanatic effects.

There are two results of diffractive anisoplanatism that need to be considered in tracker design and analysis. The first is a residual jitter that we incur, even assuming an ideal geometry and a perfect tracker with no noise or latency. The second is the frequency f_{S} at which the PSDs for differential jitter and uncorrected scoring-beam jitter cross; above this frequency, attempts to correct scoring-beam jitter with measured beacon tilt will increase jitter on target. In addition to these specific conclusions about diffractive anisoplanatism, we have described how tracker design constraints fall into practical or fundamental limitations, and can address either the desirability or possibility of jitter reduction. This framework should help in considering the place of diffractive anisoplanatism, a fundamental limitation on the possibility of jitter reduction, amongst all the other considerations when designing and analyzing tracking systems.

This page intentionally left blank.

REFERENCES

[1] P.H. Merritt, S. Peterson, R. Telgarsky, S.D. O'Keefe, R. Pringle, et al., "Performance of tracking algorithms under airborne turbulence," *Proc. SPIE* 4376, 99–106 (2001).

[2] P.H. Merritt, S. Peterson, R. Telgarsky, R. Pringle, R.L. Brunson, et al., "Limitation on the bandwidth of tracking through the atmosphere," *Proc. SPIE* 4724, 37–44 (2002).

[3] P.H. Merritt, *Beam Control for Laser Systems*, DEPS (2012).

[4] J.P. Siegenthaler, *Guidelines for Adaptive-Optic Correction Based on Aperture Filtration*, Ph.D. thesis, University of Notre Dame (2008).

[5] S.E.J. Shaw and E.M. Tomlinson, "Analytic propagation variances and PSDs from a wave-optics perspective," MIT Lincoln Laboratory, Special Report 82-1009 (2018).

[6] M.C. Roggemann and B. Welch, *Imaging through Turbulence*, CRC Press (1996).

[7] G.A. Tyler, "Bandwidth considerations for tracking through turbulence," *JOSA A* 11(1), 358–367 (1994).

[8] D.P. Greenwood, "Bandwidth specification for adaptive optics systems," *J. Opt. Soc. Am.* 67(3), 390–393 (1977).

[9] H.T. Yura and M.T. Tavis, "Centroid anisoplanatism," *JOSA A* 2, 765 (1985).

[10] C. Hogge and R. Butts, "Frequency spectra for the geometric representation of wavefront distortions due to atmospheric turbulence," *IEEE Transactions on Antennas and Propagation* 24(2), 144–154 (1976).

[11] R.J. Sasiela, *Electromagnetic Wave Propagation in Turbulence*, SPIE Press, 2nd ed. (2007).

REPORT DOCUMENTATION PAGE

Form Approved
OMB No. 0704-0188

1. REPORT DATE *(DD-MM-YYYY)*	2. REPORT TYPE	3. DATES COVERED *(From - To)*
26-09-2018	Project Report	

4. TITLE AND SUBTITLE

Diffractive Anisoplanatism and Tracker Bandwidth Limitations

5a. CONTRACT NUMBER
FA8721-05-C-0002 &/or FA8702-15-D-0001

5b. GRANT NUMBER

5c. PROGRAM ELEMENT NUMBER

6. AUTHOR(S)

S.E.J. Shaw, E.M. Tomlinson

5d. PROJECT NUMBER
1672-41

5e. TASK NUMBER

5f. WORK UNIT NUMBER

7. PERFORMING ORGANIZATION NAME(S) AND ADDRESS(ES)

MIT Lincoln Laboratory
244 Wood Street
Lexington, MA 02421-6426

8. PERFORMING ORGANIZATION REPORT NUMBER

82-1010

9. SPONSORING / MONITORING AGENCY NAME(S) AND ADDRESS(ES)

Joint Directed Energy Transition Office
801 University Boulevard, SE, Suite 209
Albuquerque, NM 87106

10. SPONSOR/MONITOR'S ACRONYM(S)
DE-JTO

11. SPONSOR/MONITOR'S REPORT NUMBER(S)

12. DISTRIBUTION / AVAILABILITY STATEMENT

Approved for public release: distribution unlimited.

13. SUPPLEMENTARY NOTES

14. ABSTRACT

This report develops the concept of \diffractive anisoplanatism," a previously omitted effect that places fundamental limitations on tracker performance for directed-energy applications. Diffractive anisoplanatism comprises two effects: fist, that diffraction causes the conversion of phase to amplitude on the beacon light used to drive a tracker, effectively hiding some atmospheric phase from tilt measurements; second, that diffraction causes a scoring beam propagating to the target to spread into regions outside of the geometric cone sampled by the beacon. These two effects result in a loss of reciprocity between the two beams, such that using the beacon tilt to correct the scoring-beam motion will not drive that motion to zero as conventional wisdom would dictate. This is true even in an idealized situation with no spatial offsets, no latency, no noise or errors, infinite bandwidth, and no time-of-fight delays. Further, this loss of reciprocity worsens as frequency increases, such that our attempts to correct scoring-beam jitter above a scenario-dependent frequency fs will actually make the jitter on target worse.

15. SUBJECT TERMS

16. SECURITY CLASSIFICATION OF:			17. LIMITATION OF ABSTRACT	18. NUMBER OF PAGES	19a. NAME OF RESPONSIBLE PERSON
a. REPORT	b. ABSTRACT	c. THIS PAGE			19b. TELEPHONE NUMBER *(include area code)*
Unclassified	Unclassified	Unclassified	Same as report	30	